Frequency-comb spectroscopy of the D_1 line in laser-cooled rubidium

M. Maric, J. J. McFerran, and A. N. Luiten
Frequency Standards and Metrology, School of Physics, The University of Western Australia, 35 Stirling Highway, Crawley WA 6009, Australia

(Received 18 September 2007; published 7 March 2008)

We have used an optical frequency comb referenced to coordinated universal time (UTC) to perform spectroscopic measurements of the D_1 transition in laser-cooled ^{85}Rb and ^{87}Rb. Our measurements of the optical frequencies have uncertainties of 28 kHz for ^{85}Rb and 79 kHz for ^{87}Rb. These measurements were used to calculate the magnetic dipole constant $A(^2P_{1/2})$ for ^{85}Rb and ^{87}Rb with similar ranges of uncertainty. Previously, $A(^2P_{1/2})$ for these isotopes was determined with a stated 7–15 kHz uncertainty level; however, there is a large discrepancy, 140 kHz for ^{85}Rb and 2.2 MHz for ^{87}Rb, between the two apparently most precise measurements. Our transition frequency measurements, which avoid saturated absorption spectroscopy and transfer resonator systematics, help resolve this disagreement.

DOI: 10.1103/PhysRevA.77.032502 PACS number(s): 32.30.−r, 32.10.Fn, 42.62.Fi, 06.30.Ft

I. INTRODUCTION

Spectroscopy has traditionally played an important role in stringently testing our understanding of both the microscopic and macroscopic world. As methods of atomic-species manipulation and interaction become more refined, the uncertainty in evaluating transition line centers has improved dramatically. This has led to a number of contemporary tests of fundamental physics through spectroscopic means. For example: (i) the precision measurements of frequency standards placing constraints on the temporal drift rates of fundamental constants, such as the fine structure constant, α [1–4], (ii) the rigorous scrutinizing of quantum electrodynamics (QED) when α determinations from the measured electron magnetic moment [5] are compared with QED calculation-free measurements of α (the latter involving many branches of laser spectroscopy) [6–8], and (iii) the increased sensitivity searches for an electron electric dipole moment in pursuit of new physics [9]. In some circumstances laboratory based spectroscopy can play an inadvertent role in testing the fundamentals of physics. While the work here is not specific to this cause, it is prudent that such a commonly studied atom, Rb, be carefully characterized in order to eliminate the possibility of any unforeseen issues.

Recently, several groups have reported measurements of the optical frequencies of the D_1 line in Rb as well as values for the magnetic dipole constant $A(^2P_{1/2})$ which determines the hyperfine splitting within the D_1 manifold [10–12]. There are strong discrepancies in the measurements presented by these groups. For example, the $A(^2P_{1/2})$ measurements of Banerjee *et al.* [11] and Das *et al.* [12] agree with the long standing measurement by Beacham *et al.* [13], but they are inconsistent with the those of Barwood *et al.* [10]. In the particular case of ^{87}Rb the magnitude of the disagreement is 130 times larger than the combined uncertainty of the two measurements [10,12]. All past spectroscopic measurements of the D_1 line have used room temperature gas cells and saturated absorption spectroscopy (SAS) as the basis of their approach. Along with possible systematic error sources associated with SAS, the authors of [10] and [11] also had to contend with characterizing and calibrating their transfer resonators in order to measure optical frequencies of the transitions involved. In contrast, in this paper we have used a femtosecond-laser based optical frequency comb and a Rb magneto-optical trap (MOT) in order to perform spectroscopy on the D_1 line of ^{85}Rb and ^{87}Rb and measure the optical frequencies of the transitions and their hyperfine intervals. The use of much slower atoms substantially reduces errors associated with Doppler shifts and relative alignment of optical and atomic beams.

II. EXPERIMENTAL SETUP

A schematic of the atomic energy levels and lasers involved in our experiment is shown in Fig. 1. We produce 10^7 cold Rb atoms by a standard six-beam MOT with a residual temperature of about 100 μK. The MOT uses a total of 30 mW of light tuned to the $|5\,^2S_{1/2},F=3(2)\rangle \rightarrow 5\,^2P_{3/2},F'=4(3)\rangle$ transition for ^{85}Rb (^{87}Rb) in 1 cm^2 beams and 5 mW

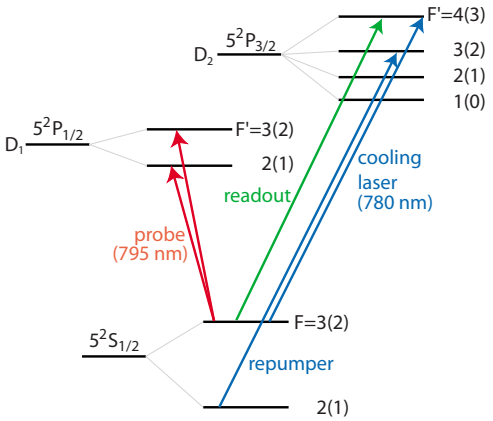

FIG. 1. (Color online) Schematic of the energy levels involved in the experiment. The monolithic block resonator (MBR) probe is swept across the D_1 states and the readout laser measures the number of atoms that remain in the initial state by interrogating the $|5\,^2S_{1/2},F=3(2)\rangle \rightarrow |5\,^2P_{3/2},F'=4(3)\rangle$ transition. The F and F' numbers outside and inside the brackets indicate the values for ^{85}Rb and ^{87}Rb, respectively.

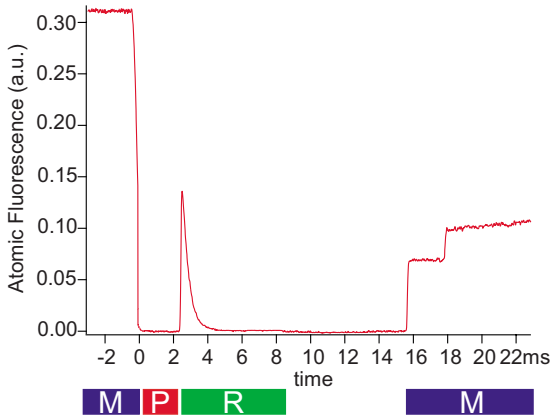

FIG. 2. (Color online) Cold atom interrogation sequence. The MOT fields (denoted by M): the magnetic field, the cooling laser, and the repumper are switched off first. The probe laser (p) is then turned on, followed by the readout laser (r). At the end of the complete sequence the MOT light fields are switched on again at 16 ms and the MOT is reloaded.

of repumping light to depopulate the $|5\ ^2S_{1/2}, F=2(1)\rangle$ state. The MOT lasers, as well as the readout laser to be described below, are all extended cavity diode laser (ECDL) systems in Littrow configuration.

We use three pairs of Helmholtz coils aligned along orthogonal axes to actively compensate for the spurious magnetic fields in the trapping region, of which the Earth's magnetic field dominates. The resolution of the current setting in the coils limits the smallest magnetic field increment to 4.8 mG, which grants a maximum 100-fold reduction of the Earth's magnetic field. When the quadrupole field is switched off and the atoms are transferred into a molasses they are no longer confined to the zero in the magnetic field. In fact, the atoms will be cooled to a finite drift velocity at which the Doppler shift compensates for the energy level shift due to the residual magnetic field [14]. We monitor the atom cloud expansion from two orthogonal directions aiming to ensure a uniform expansion and no translation of the atoms as the MOT magnetic field gradient is switched off, similar to the procedure used by Snadden *et al.* [15]. We estimate that the sensitivity of this method allows a factor of 30 reduction in the stray magnetic fields resulting in the residual magnetic field of below 15 mG.

After the cold atom sample is prepared, the MOT fields are terminated and the probe beam is switched on (see Fig. 2). This π-polarized probe beam is used to deplete atoms from the MOT prepared state, i.e., $|5\ ^2S_{1/2}, F=3(2)\rangle$. The polarization purity of the probe laser is ensured by a Glan-Taylor prism mounted at the probe laser input port of the MOT chamber. Our spectroscopic measurement is based on measuring the probe laser frequency dependence of this depletion, similar to the approach described in Ref. [16]. We use a counterpropagating probe configuration in order to minimize the mechanical effects of the probe on the cold atoms as well as to reduce sensitivity to any asymmetric expansion of the atomic cloud after its release from the MOT. Depending on the probe frequency there will be a reduction in the initial state population via optical pumping to the nonresonant ground state $|5\ ^2S_{1/2}, F=2(1)\rangle$. After a fixed interrogation time ($\sim$2 ms) the probe is switched off. The readout laser then measures the number of atoms that remain in the initial state via the closed cooling transition $|5\ ^2S_{1/2}, F=3(2)\rangle \rightarrow |5\ ^2P_{3/2}, F'=4(3)\rangle$. The data acquisition system measures this fluorescence using a Hamamatsu R6357 infrared enhanced photomultiplier tube (PMT). The fluorescent signal shows a rapid increase as the intensity of the readout light is ramped up, followed by a relatively slow exponential decay as the atoms are pumped away via off-resonant excitation to $|5\ ^2P_{3/2}, F'=3(2)\rangle$ and subsequent decay to $|5\ ^2S_{1/2}, F=2(1)\rangle$ after which they no longer interact with the readout laser (see Fig. 2). This signal is integrated in time and the integrated signal is strictly proportional to the number of atoms that remained in the initial state after exposure to the probe light. The raw integration result is also normalized to the initial atom number in the MOT, which is derived from the fluorescence measurement of the MOT prior to atom release. The frequency of the probe laser is then incremented, the MOT is reloaded, and the interrogation sequence is repeated. The advantage of this technique is that while the atoms interact with a very weak probe signal, we are able to measure the outcome of the interaction using a strong and nearly closed transition which amplifies the signal to noise ratio of the measurement. In addition, the final atom number derived from this integrated fluorescence is insensitive to small fluctuations in the power or frequency of the readout laser.

To carry out our frequency measurements we use a femtosecond-laser based self-referenced frequency comb as shown in Fig. 3. By convention, the frequency of each mode of the comb is expressed as $f_n = nf_{rep} + f_0$ [17]. The comb offset frequency f_0 is stabilized using the standard f-$2f$ interferometer [17]. We count and record f_0 as a consistency check and to ensure that the control system is working properly. The pulse repetition rate f_{rep} is stabilized by phase-locking the 10th harmonic of f_{rep} to a low noise tunable synthesizer (Agilent E8257C). The frequency accuracy of the whole system is ensured by steering the synthesizer that stabilizes f_{rep} and the f_0 frequency counter with a local H maser. The maser is continually compared by common-view GPS time and frequency transfer to UTC(AUS), Australia's realization of coordinated universal time (UTC), maintained at the National Measurement Institute (NMI) in Sydney. Frequency measurements can thus be referenced via the maser and UTC(AUS) to UTC. A more detailed description of our frequency comb is available in Refs. [18,19].

The probe laser is based around a commercial tunable cw Ti:sapphire system (Coherent MBR-110E) with a measured frequency instability of 0.5 MHz over time scales of a few seconds (see Fig. 4). For these spectroscopic studies we aimed for a fractional uncertainty of 10^{-10} and so the free-running performance of this device was insufficient to meet this goal. In order to improve the precision of the frequency measurement, the laser was stabilized by locking its frequency at a user-defined offset to one of modes in the highly stable frequency comb. The light of the MBR heterodynes with the nearest mode of the frequency comb when the light signals are combined. The resulting beat signal was supplied

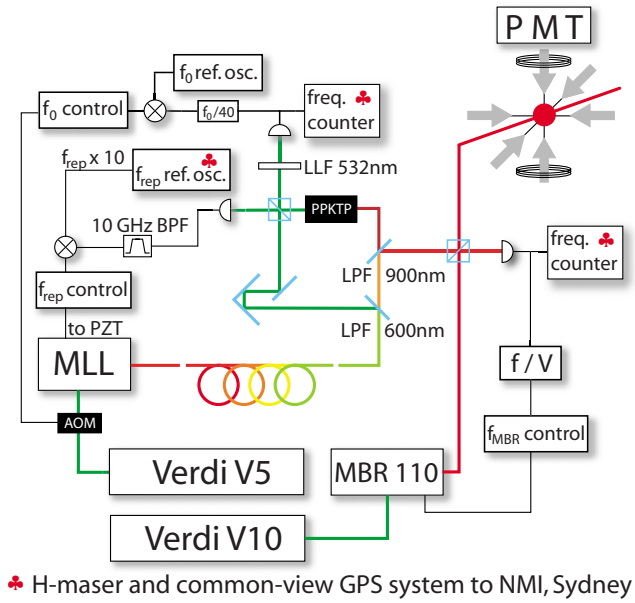

FIG. 3. (Color online) Experimental setup of the self-referenced frequency comb and the Rb MOT with the thin and thick lines depicting electrical signals and light paths, respectively. The f_{rep} local oscillator and the two frequency counters are referenced UTC(AUS) at NMI via a H maser and the common view GPS system. Mode-locked laser (MLL), frequency to voltage converter (f/V), comb offset frequency (f_0), pulse repetition rate (f_{rep}).

to a frequency-locked loop (FLL) circuit [20] in order to derive a correction signal that can be used to hold this difference frequency constant. We chose to use a FLL for this application, rather than a phase-locked loop (PLL), because the low bandwidth of the external modulation port of the MBR-110 laser does not allow sufficiently fast feedback to suppress the phase fluctuations of the laser to below 1 rad. In the circumstances of high levels of residual phase noise a PLL cannot be relied upon to provide an appropriate correction signal without the inclusion of additional and more complex electronics [20]. The fractional frequency fluctuations of the probe laser with the FLL in place were around 3×10^{-12} (1 kHz) over 0.1–1 s time scales (lower trace in Fig. 4). Since the H-maser stabilized comb is predicted to be below this, the residual beat fluctuations determines the instability of the probe laser. At parts in 10^{-12} it is not a dominant source of uncertainty in the Rb frequency measurements. The frequency of the probe laser is swept through the atomic resonances by changing f_{rep} through the data acquisition system. Due to the finite gain of the FLL, the beat frequency between the probe and the comb drifts as the f_{rep} is scanned. Therefore throughout the measurement, we count and record both f_{rep} and this beat frequency to guarantee that this long term drift does not affect the accuracy of our frequency measurement.

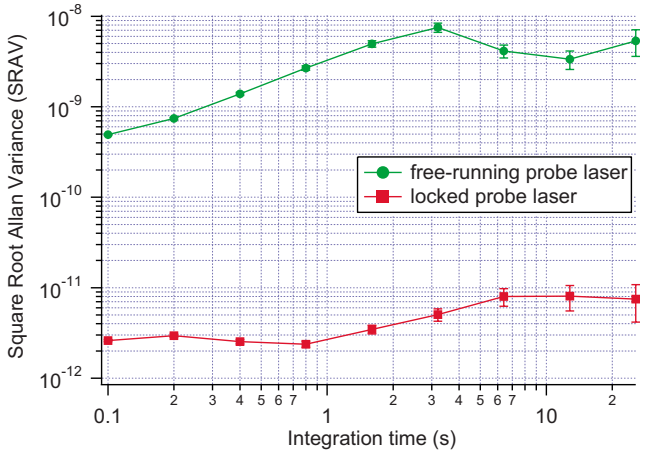

FIG. 4. (Color online) Frequency stability of the free-running and the frequency stabilized probe laser.

III. MEASUREMENT AND ANALYSIS

The optical frequency of the probe laser can be expressed as

$$f_{\mathrm{PL}} = nf_{\mathrm{rep}} \pm f_0 \pm f_{\mathrm{MBR}}, \tag{1}$$

where n is the comb mode number to which the probe laser has been locked, and the f_{MBR} is the beat frequency between the probe laser and the nearest comb mode. The mode number n is uniquely determined using previous frequency measurements of the optical frequencies in question [10,11,21]. The high f_{rep} of around 1 GHz of our fs laser allows for unambiguous determination of n. The sign in front of the f_0 term is determined by scanning the probe across a line, changing the value of f_0, and seeing in which direction the atomic line resonance shifts. A similar procedure is used to determine the sign preceding the f_{MBR} term. Typically, the values used to scan the probe across the $|5\,^2S_{1/2}, F=3\rangle \rightarrow |5\,^2P_{1/2}, F'=3\rangle$ transition in ^{85}Rb are $n=372\,770$, $f_0=-184$ MHz, $f_{\mathrm{MBR}}=-7.02$ MHz and the f_{rep} is scanned over a 100-Hz interval centered at approximately 1.011 633 078 GHz.

A frequency dependent exponential decay function is fitted to the fluorescence profile produced by scanning the probe laser,

$$N_0 \exp\left(\frac{A}{1+[4(\nu-\nu_0)^2/\Gamma^2]}\right), \tag{2}$$

with center frequency (ν_0), linewidth (Γ) and amplitude (A) as the free parameters. We have verified this expected functional form by a density matrix model of the experimental situation. A trace of the ^{85}Rb spectra is shown in Fig. 5. A sequence of measurements at different optical intensities shows that the zero power extrapolated linewidth is 6.5 ± 0.3 MHz which is in reasonable agreement with the expected linewidth of 5.7 MHz [22]. We believe that some of this discrepancy is explained by the residual linewidth of the probe laser which is a combination of the free running linewidth of probe laser, reduced by the gain of the FLL with a 1-kHz bandwidth, together with the high frequency noise of the frequency comb that is transferred onto the probe laser via the FLL. The high frequency noise on the frequency comb principally arises from the f_{rep} lock which imposes the microwave synthesizer noise onto the frequency-comb modes in the optical domain. Our conservative estimate of

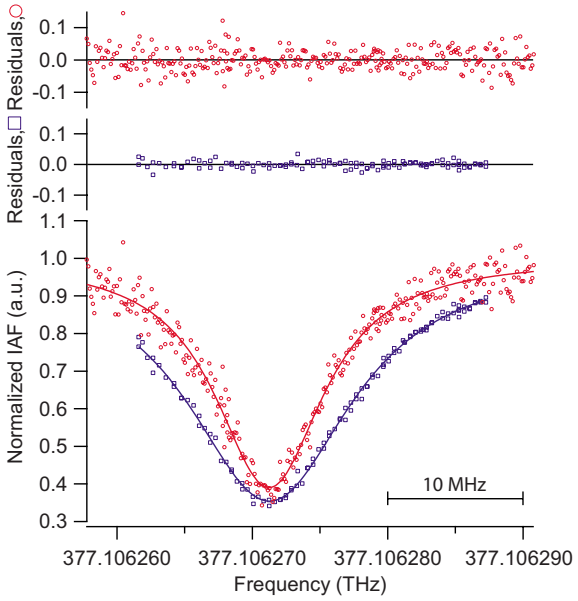

FIG. 5. (Color online) Normalized integrated atomic fluorescence (IAF) of the $|5\,^2S_{1/2}, F=3\rangle \rightarrow |5\,^2P_{1/2}, F'=3\rangle$ transition in ^{85}Rb recorded at two different probe laser intensities (circles: 60 μW/cm^2; squares: 140 μW/cm^2) with line fits to the data and their residuals. The fitted linewidths are 7.7 MHz and 11.3 MHz, respectively.

the probe laser linewidth is around 300 kHz and it would appear reasonable to conclude that measured linewidth is to some degree a combination of the probe laser linewidth and the natural linewidth.

A. Uncertainty budget

There are several sources of possible systematic shifts and uncertainties which limit the ultimate precision of the measured atomic line center frequencies, as shown in Table I.

TABLE I. Sources and magnitudes of various error budget components and corrections. All units are in kHz.

Source	Correction	Uncertainty
ac Stark shift		
^{85}Rb		15
^{87}Rb		6.5
Zeeman shift		15
Recoil shift	−3.6	
Velocity redistribution		0.7
Probe laser frequency		1.1
UTC correction	0.377	0.04
Statistical error of line fit		
^{85}Rb		18
^{87}Rb		77
	Sum	Sum in quadrature
^{85}Rb	−3.223	28
^{87}Rb	−3.223	79

TABLE II. Frequency measurements of the D_1 line of ^{85}Rb and ^{87}Rb. Femtosecond laser comb (fs comb), Interferometric measurement (INT), direct frequency-comb spectroscopy (DFCS). An offset of 377 100 000 MHz is subtracted for convenience.

Isotope	Transition $F \rightarrow F'$	Frequency[a] (MHz)	Type of measurement	Source
^{85}Rb	$3 \rightarrow 2$	5909.777 (28)	fs comb	this work
		5910.105(133)	INT	[10]
		5909.371 (7)	INT	[11]
	$3 \rightarrow 3$	6271.276 (28)	fs comb	this work
		6271.600(133)	INT	[10]
		6271.848 (7)	INT	[11]
^{87}Rb	$2 \rightarrow 1$	4389.803 (79)	fs comb	this work
		4390.053(133)	INT	[10]
		5909.371 (7)	INT	[11]
	$2 \rightarrow 2$	5206.462 (79)	fs comb	this work
		5206.705(133)	INT	[10]
		5205.365 (7)	INT	[11]
		5206.939(179)	DFCS two photon	[21]
		5206.563(184)	DFCS one photon	[24]

[a]Frequencies and $1-\sigma$ uncertainties for Refs. [10,11] calculated from information provided within.

The first item in the error budget is the ac Stark shift due to the off-resonant coupling of the probe light to other hyperfine components of the D_1 line. The hyperfine components of the D_1 line of both isotopes are separated by relatively large amounts which allows the ac Stark shift to be adequately quantified using the expression [23]

$$\delta^{\mathrm{ac}} \approx \frac{1}{2}(\Delta \pm \sqrt{\Delta^2 + \Omega^2}), \tag{3}$$

where $2\pi\Omega$ is the Rabi frequency and Δ is the frequency separation between the hyperfine components. We calculate the maximum possible size of the ac Stark shift using twice the interrogating power of a single beam in order to account for the counterpropagating probe configuration. The difference in the size of the effect for the two isotopes is due to the larger hyperfine splitting in ^{87}Rb. The sequence of measurements at different intensities resulted in a frequency shift of $17(\pm 170)$ Hz/(μW/cm^2) compared to the expected value of 100 Hz/(μW/cm^2) for ^{85}Rb and 47 Hz/(μW/cm^2) for ^{87}Rb. We therefore do not apply the ac Stark shift as a correction, but instead allow an uncertainty of the maximum calculated shift for the experimental conditions.

Photon recoil causes two systematic frequency shifts [23]; the first comes from the shift in the atomic absorption line by the recoil energy $E_r = 2\pi\hbar \times 3.6$ kHz, and we correct for this by subtracting it from the measured line center frequencies. The second contribution of the photon recoil is associated with the change of atomic velocity after an absorption-emission cycle, which for the D_1 line is about 7.2 kHz for both isotopes. During the interrogation of the cold atom sample we set the probe laser intensity so that the initial

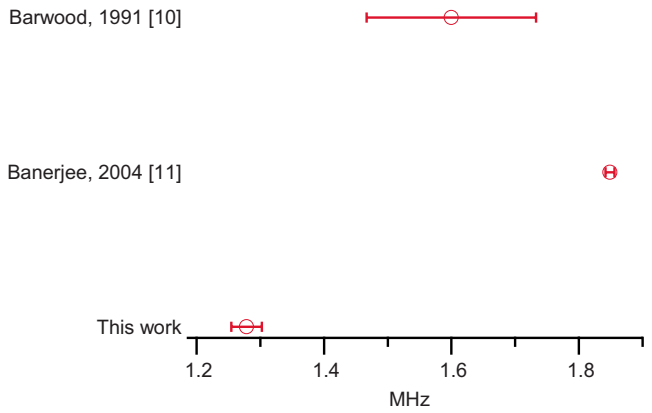

FIG. 6. (Color online) Optical frequency measurements of the $|5\ ^2S_{1/2}, F=3\rangle \rightarrow |5\ ^2P_{1/2}, F'=3\rangle$ transition in ^{85}Rb. An offset of 377 106 270 MHz is subtracted for convenience.

MOT population is halved when the probe laser is at the center of resonance as depicted in Fig. 5. Under such conditions every atom on average interacts with only one photon because they are efficiently optically pumped into the nonresonant ground state. Combined with the use of a retroreflected counterpropagating probe configuration we expect that the recoil shift associated with the atomic velocity redistribution in a absorption-emission cycle is not significant in our experiment. However, we include 10% of one photon recoil worth of uncertainty due to a potentially small imbalance in the intensity of the probe beams. The stray magnetic field of about 15 mG results in the uncertainty of 15 kHz in the optical frequencies of the D_1 lines measured.

We also note that the optical pumping between Zeeman sublevels is not a significant source of frequency shift because there are no cycling transitions interrogated and the atoms are interrogated by the π-polarized probe laser. Therefore most atoms leave the atomic population resonant with the probe laser after one or two absorption-emission cycles.

The probe laser frequency measurement error is due to the residual frequency fluctuations of the probe laser with respect to the frequency comb. The fractional frequency

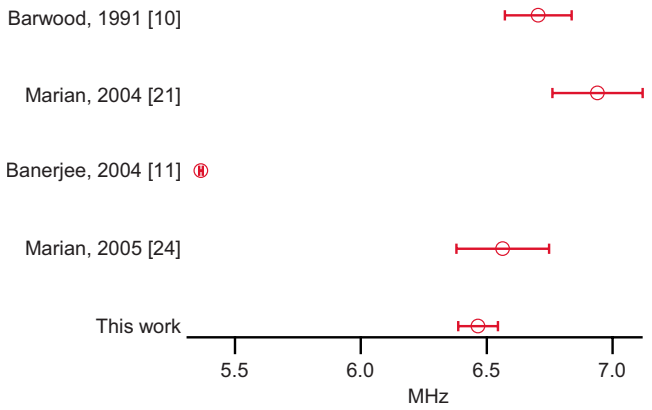

FIG. 7. (Color online) Optical frequency measurements of the $|5\ ^2S_{1/2}, F=2\rangle \rightarrow |5\ ^2P_{1/2}, F'=2\rangle$ transition in ^{87}Rb. An offset of 377 105 200 MHz is subtracted for convenience.

TABLE III. The magnetic dipole constant $A(^2P_{1/2})$ for ^{85}Rb and ^{87}Rb. All units are in MHz.

^{85}Rb $A(^2P_{1/2})$	^{87}Rb $A(^2P_{1/2})$	Source
120.72(17)	406.2 (8)	[13]
120.499(10)	408.326(15)	[10]
120.64(2)	406.147(15)	[11]
120.645(5)	406.119 (7)	[12]
120.500(13)	408.330(56)	this work

instability of 3×10^{-12} corresponds to approximately 1.1 kHz at the D_1 line frequency. The correction for the rate of the H maser against UTC is calculated from two terms: the maser rate against UTC(AUS), which is obtained from a linear regression to common-view GPS transfer data, and the rate of UTC(AUS) against UTC, published monthly in *Circular T* by the International Bureau of Weights and Measures (BIPM). The first term corresponds to a fractional frequency offset of approximately 1×10^{-12}; the second is of order 10^{-14} and therefore negligible.

The last item in the error budget is the statistical error in the line fit. It is the result of the achieved signal to noise ratio and it includes all other noise sources such as the noise in the number of trapped atoms, PMT detection, probe laser power fluctuations.

IV. RESULTS

The results of our frequency measurements are collected and compared to values available in literature in Table II and the $F=3\rightarrow F'=3$ and $F=2\rightarrow F'=2$ transitions for ^{85}Rb and ^{87}Rb, respectively, are shown graphically in Figs. 6 and 7. Our measurements agree reasonably well with those of [10,21,24] while there seems to be some significant disagreement with the results reported in [11]. All measurement uncertainties are expressed as $1-\sigma$ of the mean.

The energy splitting E_F due to the magnetic dipole and electric quadrupole interactions between the electrons and the nucleus which give rise to the hyperfine level structure is given by [25]

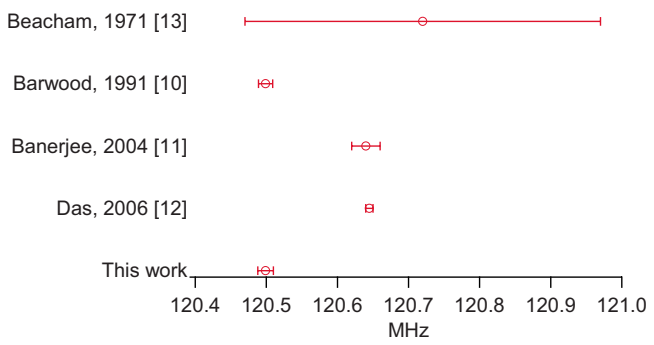

FIG. 8. (Color online) Magnetic dipole constant $A\ ^2P_{1/2}$ for ^{85}Rb.

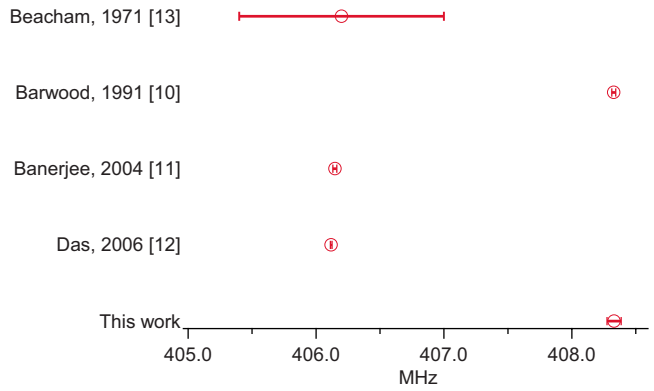

FIG. 9. (Color online) Magnetic dipole constant $A\,^2P_{1/2}$ for ^{87}Rb.

$$E_F = \frac{1}{2}hAK + hB\frac{(3/2)K(K+1) - 2I(I+1)J(J+1)}{2I(2I-1)2J(2J-1)}, \quad (4)$$

where $K=F(F+1)-I(I+1)-J(J+1)$ and A and B are the magnetic dipole and electric quadrupole constants, respectively. In the case of the D_1 line the electric quadrupole interaction is not present and therefore B is identically zero. We have used our frequency measurements and Eq. (4) to calculate the values of the magnetic dipole constants $A(^2P_{1/2})$ for both isotopes. Their values and comparisons with the values available in literature are shown in Table III and Figs. 8 and 9. Our results are in good agreement with those of Barwood *et al.* [10] in the case of both isotopes while we could not reproduce the results quoted in Refs. [11,12].

The fine structure interval can also be calculated by combining our values of the $A(^2P_{1/2})$ constants with the values of $A(^2S_{1/2})$ from the best available microwave measurements of the ground state hyperfine intervals from Refs. [25,26]. for ^{85}Rb and ^{87}Rb, respectively. These results are displayed in Table IV. In this case satisfactory agreement is seen between all past measurements.

TABLE IV. Fine structure splittings (FSS) and the isotope shift (IS) for ^{85}Rb and ^{87}Rb. An offset of 377 100 000 MHz is subtracted from FSS values for convenience. All units are in MHz.

FSS (^{85}Rb)	FSS (^{87}Rb)	IS	Source
7385.544(26)	7463.226(98)	77.682(102)	this work
7385.675(50)	7463.376(50)	77.701 (70)	[11]
		77.583 (12)	[10]

V. CONCLUSION

We have measured the optical frequencies of the $|5\,^2S_{1/2},F=3\rangle \rightarrow |5\,^2P_{1/2},F'=2,3\rangle$ transitions in ^{85}Rb and $|5\,^2S_{1/2},F=2\rangle \rightarrow |5\,^2P_{1/2},F'=1,2\rangle$ in ^{87}Rb and calculated the respective values of the magnetic dipole constant $A(^2P_{1/2})$. To the best of our knowledge these are the first reported frequency-comb based measurements of the $|5\,^2S_{1/2},F=3\rangle \rightarrow |5\,^2P_{1/2},F'=2,3\rangle$ transitions in ^{85}Rb. We also combined our measurements with the most accurate available microwave measurements of the hyperfine ground state frequency interval in order to calculate the size of the hyperfine-free value of the fine structure interval of the D_1 line of ^{85}Rb and ^{87}Rb and their respective isotope shift. Our measurements show a consistency with the past measurements of Barwood *et al.* [10] and Marian *et al.* [21,24] but are not consistent with other recently published measurements by Banerjee *et al.* [11] and Das *et al.* [12].

The authors would like to thank Bruce Warrington of the National Measurement Institute, Australia for his work on calculating the UTC corrections and for proofreading this manuscript as well as Mike Tobar and John Hartnett for setting up the common-view GPS link between UWA and NMI. We would also like to thank the Australian Research Council for funding and supporting this work.

[1] T. Fortier *et al.*, Phys. Rev. Lett. **98**, 070801 (2007).
[2] M. Fischer *et al.*, Phys. Rev. Lett. **92**, 230802 (2004).
[3] E. Peik, B. Lipphardt, H. Schnatz, T. Schneider, C. Tamm, and S. Karshenboim, Phys. Rev. Lett. **93**, 170801 (2004).
[4] E. R. Hudson, H. J. Lewandowski, B. C. Sawyer, and J. Ye, Phys. Rev. Lett. **96**, 143004 (2006).
[5] B. Odom, D. Hanneke, B. D'Urso, and G. Gabrielse, Phys. Rev. Lett. **97**, 030801 (2006).
[6] V. Gerginov, K. Calkins, C. Tanner, J. McFerran, S. Diddams, A. Bartels, and L. Hollberg, Phys. Rev. A **73**, 032504 (2006).
[7] H. Muller, S.-W. Chiow, Q. Long, C. Vo, and S. Chu, Appl. Phys. B: Lasers Opt. **B84**, 633 (2006).
[8] P. Clade, E. de Mirandes, M. Cadoret, S. Guellati-Khelifa, C. Schwob, F. Nez, L. Julien, and F. Biraben, Phys. Rev. Lett. **96**, 033001 (2006).
[9] J. Hudson, H. Ashworth, D. Kara, M. Tarbutt, B. Sauer, and E. Hinds, Phys. Rev. A **76**, 033410 (2007).
[10] G. Barwood, P. Gill, and W. R. C. Rowley, Appl. Phys. B: Lasers Opt. **53**, 142 (1991).
[11] A. Banerjee, D. Das, and V. Natarajan, Europhys. Lett. **65**, 172 (2004).
[12] D. Das and V. Natarajan, Eur. Phys. J. D **37**, 313 (2006).
[13] J. R. Beacham and K. L. Andrews, J. Opt. Soc. Am. **61**, 231 (1971).
[14] H. Metcalf and P. van der Straten, Phys. Rep. **244**, 203 (1994).
[15] M. Snadden, A. Bell, E. Riis, and A. Ferguson, Opt. Commun. **125**, 70 (1996).
[16] I. Courtillot, A. Quessada, R. P. Kovacich, A. Brusch, D. Kolker, J.-J. Zondy, G. D. Rovera, and P. Lemonde, Phys. Rev. A **68**, 030501(R) (2003).
[17] S. T. Cundiff and J. Ye, Rev. Mod. Phys. **75**, 325 (2003).
[18] J. J. McFerran, M. Maric, and A. N. Luiten, Appl. Phys. B: Lasers Opt. **79**, 39 (2004).
[19] J. J. McFerran, S. T. Dawkins, P. L. Stanwix, M. E. Tobar, and

A. N. Luiten, Opt. Express **14**, 4316 (2006).
[20] T. Stace, R. Kovacich, and A. N. Luiten, Meas. Sci. Technol. **9**, 1635 (1998).
[21] A. Marian, M. C. Stowe, J. R. Lawall, D. Felinto, and J. Ye, Science **306**, 2063 (2004).
[22] U. Volz and H. Schmoranzer, Phys. Scr. **T65**, 48 (1996).
[23] S. Falke, E. Tiemann, C. Lisdat, H. Schnatz, and G. Grosche, Phys. Rev. A **74**, 032503 (2006).
[24] A. Marian, Ph.D. thesis, JILA, University of Colorado, Boulder, CO, 2005.
[25] E. Arimondo, M. Inguscio, and P. Violino, Rev. Mod. Phys. **49**, 31 (1977).
[26] S. Bize, Y. Sortais, M. S. Santos, C. Manache, A. Clarion, and C. Salomon, Europhys. Lett. **45**, 558 (1999).